sustainability

MDPI

Article

Multiple-Zone Synchronous Voltage Regulation and Loss Reduction Optimization of Distribution Networks Based on a Dual Rotary Phase-Shifting Transformer

Chen Shao [1], Xiangwu Yan [1,*], Yaohui Yang [1], Waseem Aslam [2], Jiaoxin Jia [1] and Jiayao Li [1]

[1] Key Laboratory of Distributed Energy Storage and Micro-Grid of Hebei Province, North China Electric Power University, Baoding 071003, China; shaochen@ncepu.edu.cn (C.S.); yangyh_ee@ncepu.edu.cn (Y.Y.); jiajx33@ncepu.edu.cn (J.J.); lijiayao@ncepu.edu.cn (J.L.)

[2] Department of Electrical, Electronics and Computer Systems, University of Sargodha (UOS), Sargodha 40100, Punjab, Pakistan; wasimevergreen@yahoo.com

* Correspondence: xiangwuy@ncepu.edu.cn; Tel.: +86-18131215880

Abstract: For the problem in which accessing a high proportion of renewable energy results in exceeding the limit in distribution network voltage, the existing regulating method experiences difficulty in considering the two-way voltage regulation and loss reduction optimization function. This study proposes a series-type dual rotary phase-shifting transformer (DRPST) based on the principle of phase volume synthesis. This transformer exhibits bidirectional voltage regulation, high reliability, and low cost. First, the topology, operating principle, and equivalent circuit of DRPST are introduced, and its simplified circuit model is established. On the basis of this model, the causes of voltage exceeding the limits are analyzed and the active distribution network model that contains DRPST is constructed. A real-time rolling two-layer optimization strategy based on DRPST is proposed. The inner layer model is solved using the multi-objective particle swarm optimization algorithm with the objective of minimizing voltage deviation and line loss. The optimal compromise solution of the Pareto solution set of the inner layer model is determined using the fuzzy subordinate degree function method. The outer model is based on the optimal compromise solution of the inner model, and the DRPST output rotor angle is controlled without deviation through double closed-loop proportional–integral regulation. Finally, the correctness and effectiveness of the proposed topology and control method are verified via simulation and experimental analysis.

Keywords: dual rotary phase-shifting transformer; active distribution grid; bidirectional voltage regulation; loss reduction optimization

Citation: Shao, C.; Yan, X.; Yang, Y.; Aslam, W.; Jia, J.; Li, J. Multiple-Zone Synchronous Voltage Regulation and Loss Reduction Optimization of Distribution Networks Based on a Dual Rotary Phase-Shifting Transformer. *Sustainability* **2024**, *16*, 1029. https://doi.org/10.3390/su16031029

Academic Editor: Pablo García Triviño

Received: 12 October 2023
Revised: 25 December 2023
Accepted: 16 January 2024
Published: 25 January 2024

1. Introduction

In an era characterized by energy crisis and environmental pollution, the research and development of renewable energy sources have been promoted and photovoltaic (PV) power occupies an important position among various renewable energy sources [1]. However, access to large-scale distributed energy sources on the user side of distribution networks and the diversification of user loads will change the traditional distribution network from a one-way to a two-way power flow, affecting the voltage distribution of the whole network and causing serious voltage crossing limits [2].

Three types of studies have been conducted for the voltage control problem of active distribution networks: on-load tap changer (OLTC) [3,4], energy storage participation [5,6], and rotary power flow controller (RPFC) [7,8] voltage regulation. In the literature [3,4], distribution network voltage control is achieved via OLTC. However, the OLTC approach exhibits the disadvantages of limited regulation capability, insufficient accuracy, and long regulation time. The literature [5,6] has studied the voltage regulation control strategy that involves the participation of energy storage systems to achieve the control of grid voltage by suppressing the fluctuation of the active power output of a PV system. However, this approach demonstrates the drawbacks of difficult site selection, investment cycle production, and high losses. RPFC is an electromagnetic flexible alternating current transmission device based on a dual rotary phase-shifting transformer (DRPST) [7,8]. It achieves flexible control of line power by controlling the relative angles of the stator and rotor of two sets of rotary phase-shifting transformers (RPSTs) and by stringing a voltage phase with continuously adjustable amplitude/angle into the line. However, given that its primary structure includes two sets of RPSTs, when RPFC is applied to the active distribution network voltage regulation scenario [9], the co-ordinated control of the two RPSTs (i.e., the two control variables) causes RPFC to exhibit the problem of slow voltage regulation and periodic oscillations when meeting the demand for continuous and frequent voltage regulation in an active distribution network [10].

The effective reduction in distribution network loss under the premise of satisfying stable voltage control is also an urgent problem in grid operation [11]. The authors of [12] designed a loss reduction optimization method for distribution networks that included smart soft switches and comprehensively considered the system network loss and charging/discharging power characteristics of electric vehicles. They then established a multi-objective optimal configuration model for smart soft switches with total loss minimization as the objective function, introduced a genetic algorithm for solving, and verified the feasibility of the proposed model and the effectiveness of the solution algorithm on the basis of the IEEE 33-node system simulation model. In [13], the authors considered the regulation capacity and cost of voltage-regulating devices, such as OLTC, distributed power supply, and capacitor bank. They also established a voltage control model based on the co-ordinated optimization of energy saving and loss reduction in distribution networks and solved it using an improved particle swarm optimization (PSO) algorithm to obtain the optimal regulation capacity of each voltage-regulating device in the current optimization period. Their simulation results showed that the model and optimization method effectively reduced system network loss and user economic loss.

In the current study, we combine the two aforementioned aspects to achieve the synchronization of safe grid operation and grid loss reduction in accordance with the literature [7,8,12,13]. First, a DRPST device based on the principle of phase synthesis is proposed. This device exhibits the characteristics of bidirectional voltage regulation, high reliability, and low cost. The topology and working principle of this device are analyzed, and a simplified circuit model of DRPST is established. Then, a real-time rolling double-layer optimization model based on DRPST is developed to address the problem of synchronous voltage regulation in multiple zones of active distribution networks. Second, an improved multi-objective PSO is used to calculate the DRPST output voltage, and a double closed-loop proportional–integral (PI) control strategy is adopted to control DRPST rotor angle in real time. The simulation is verified on MATLAB/Simulink, and the results show that DRPST can effectively reduce line loss while ensuring voltage compliance in multiple active distribution networks. Finally, a 380 V/40 kVA DRPST experimental platform is constructed to verify the effectiveness of the proposed control strategy. The simulation and experimental results indicate that DRPST is an effective supplement to the voltage regulation method for an active distribution network.

2. Topology and Working Principle of DRPST

2.1. Topology of DRPST

The topology of DRPST is depicted in Figure 1. RPST is the core component of DRPST, and two groups of RPST stator side are connected in parallel to the transmission line as excitation energy extraction winding. Meanwhile, its rotor side is connected to the transmission line after a series connection. By changing the phase sequence of the two groups of RPST stator-side wiring to receive energy, the order of the two groups of RPST series-connected measurement access voltage is changed relative to the three phase load terminals (U, V, and W). The first group of RPST access voltage order is A, B, C (positive sequence), while the second group is A, C, B (reverse sequence).

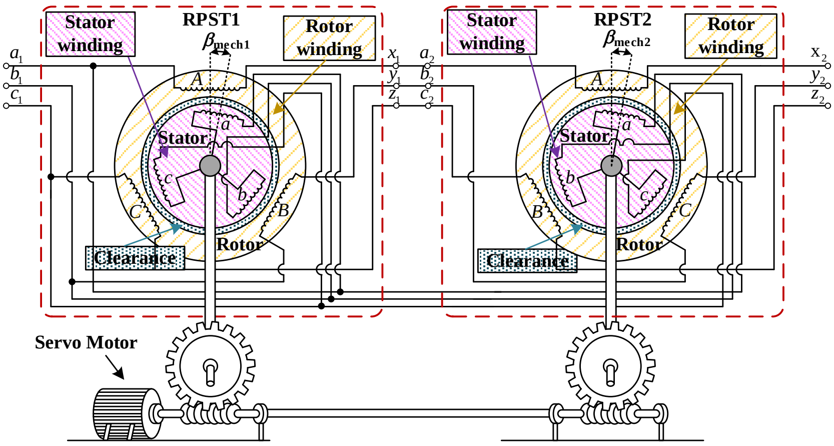

Figure 1. Topology of DRPST.

In accordance with the principle of electromagnetic induction, the rotor angle rotation of the two RPSTs is used to synthesize a rotor voltage phase with constant amplitude, opposite phase angle, and 360° adjustability. The two voltage phases are superimposed to inject a series voltage with continuously variable amplitude and the same phase angle as the original line.

2.2. Working Principle Analysis

The single-phase equivalent circuit of DRPST is shown in Figure 2, where $\boldsymbol{I}_{\mathrm{s}}$ is the system line current before connection to RPST, $\boldsymbol{I}_{\mathrm{sh}}$ is the total stator-side current, $\boldsymbol{I}_{\mathrm{s1}}$ is the rotor-side current, $\boldsymbol{U}_{\mathrm{DRPST}}$ is the voltage of the DRPST series flowing into the line, Z_{sh} is the impedance attributed to the rotor side, Z_{RPST1} and Z_{RPST2} are the impedance attributed to the stator side, and k is the DRPST voltage variation ratio size [14,15].

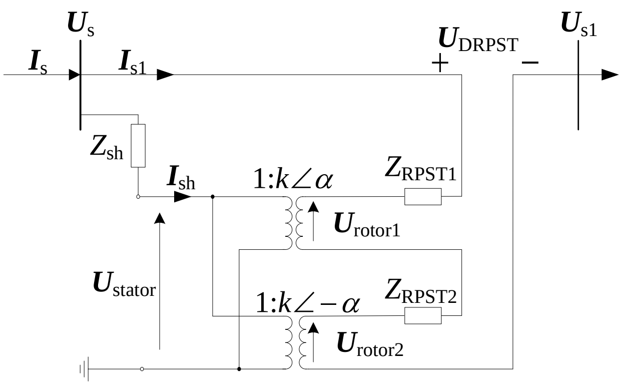

Figure 2. DRPST single-phase equivalent circuit diagram.

By analyzing the circuit in Figure 3, the following equations are obtained:

$$\boldsymbol{U}_{\mathrm{stator}} = \boldsymbol{U}_{\mathrm{s}} - \boldsymbol{I}_{\mathrm{sh}} Z_{\mathrm{sh}}, \tag{1}$$

$$\boldsymbol{U}_{\mathrm{DRPST}} = \boldsymbol{U}_{\mathrm{rotor1}} + \boldsymbol{U}_{\mathrm{rotor2}} + 2\boldsymbol{I}_{\mathrm{s1}} Z_{\mathrm{RPST}}, \tag{2}$$

$$\boldsymbol{I}_{\mathrm{s}} = \boldsymbol{I}_{\mathrm{s1}} + \boldsymbol{I}_{\mathrm{sh}}, \tag{3}$$

$$\begin{cases} \boldsymbol{U}_{\mathrm{rotor1}} = \boldsymbol{U}_{\mathrm{stator}} k\angle\alpha = (\boldsymbol{U}_{\mathrm{s}} - \boldsymbol{I}_{\mathrm{sh}} Z_{\mathrm{sh}}) k e^{\mathrm{j}\alpha} \\ \boldsymbol{U}_{\mathrm{rotor2}} = \boldsymbol{U}_{\mathrm{stator}} k\angle - \alpha = (\boldsymbol{U}_{\mathrm{s}} - \boldsymbol{I}_{\mathrm{sh}} Z_{\mathrm{sh}}) k e^{-\mathrm{j}\alpha} \end{cases}, \tag{4}$$

$$U_{\rm DRPST} = (U_{\rm sA} - I_{\rm sh}Z_{\rm sh})k\cos\alpha + 2I_{\rm s1}Z_{\rm DRPST}, \tag{5}$$

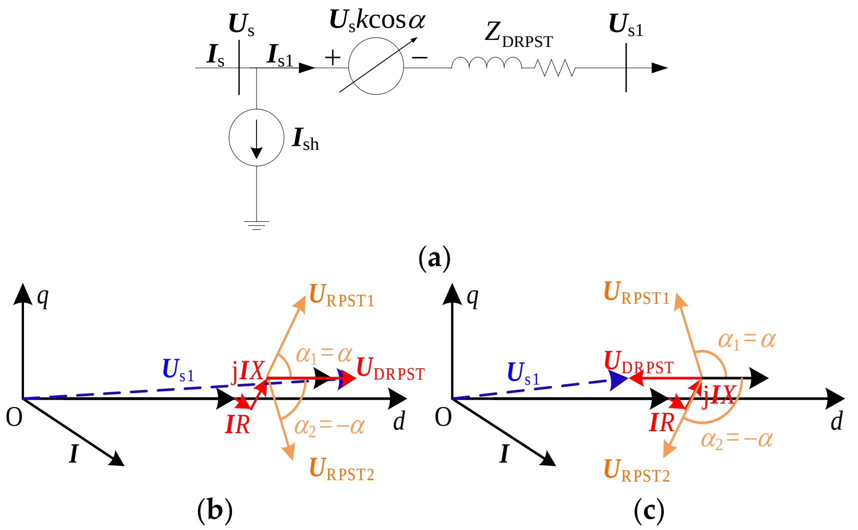

Figure 3. Simplified circuit model and voltage regulation vector diagram of DRPST. (**a**) Simplified circuit diagram of DRPST. (**b**) Regulating vector diagram of DRPST when crossing the lower limit. (**c**) Regulating vector diagram of DRPST when the upper limit is crossed.

Assuming the premise of an ideal RPST, the following equation exists at this point [16,17]:

$$U_{\rm Rotor} \cdot {I_{\rm sh}}^* = U_{\rm Stator} \cdot {I_{\rm s1}}^*, \tag{6}$$

From Equations (3), (4) and (6), the total rotor current and system line current can be calculated as:

$$\begin{cases} I_{\rm s1} = \frac{I_{\rm s}}{(1+k\cos\alpha)} \\ I_{\rm sh} = \frac{kI_{\rm s}\cos\alpha}{(1+k\cos\alpha)} \end{cases}, \tag{7}$$

By combining Equations (5) and (7), we derive:

$$U_{\rm DRPST} = U_{\rm s}k\cos\alpha - I_{\rm s}Z_{\rm DRPST}, \tag{8}$$

where:

$$Z_{\rm DRPST} = \frac{kZ_{\rm sh}k\cos^2\alpha + 2Z_{\rm RPST}}{1 + k\cos\alpha}, \tag{9}$$

Thus, the simplified circuit model of DRPST can be obtained as shown in Figure 3a. By changing the size of α, the change in size and direction of the series-controlled voltage source flowing into the line is achieved and the continuous regulation of the line voltage is completed. Let $U_{\rm DRPST}\prime = U_{\rm sA}k\cos\alpha$, the DRPST bidirectional voltage regulation vector diagram is shown in Figure 3b,c.

3. Active Distribution Network Voltage Regulation Model for Multiple Zones That Considers Line Losses

3.1. Active Distribution Network Model with DRPST for Multiple Zones

Most traditional distribution networks exhibit a radial structure, where load is distributed along the line and power under stable operating conditions is always transmitted in a single direction along the distribution network feeder; Figure 4 shows an example of a distribution network [15,16]. The active distribution network lines suffer from the problem of uncertain power magnitude and direction, which causes voltage instability and changes in voltage distribution.

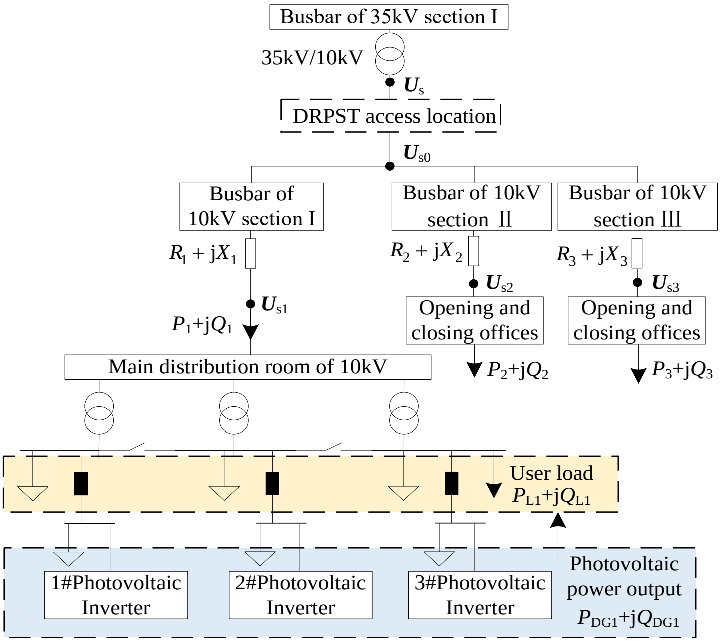

Figure 4. Active distribution grid system with distributed PV.

In the figure, $\boldsymbol{U}_{s0}$ is the 10 kV section bus voltage, $R_1 + jX_1$ is the equivalent line impedance of the 10 kV section bus I, U_{s1} is the parallel network voltage of the 10 kV section bus I, P_{Li} and Q_{Li} are the loads at node i, and P_{DGi} and Q_{DGi} are the active power and reactive power injected by the distributed PV connected to node i. At this moment, the line power of the 10 kV section bus I distribution station exists as $P_i = P_{Li} + P_{DGi}$, $Q_i = Q_{Li} + Q_{DGi}$. The voltage of each station parallel network and that of the first end of the 10 kV line are as follows:

$$U_{si} = U_{s0} - \frac{P_i R_i + Q_i X_i}{U_{s0}} \tag{10}$$

For the 10 kV distribution line with $R \gg X$, Equation (10) indicates that $P_i R_i + Q_i X_i < 0$ will lead to $U_{si} > U_{s0}$. Therefore, when the phenomenon of active power backfeeding occurs, the voltage of the parallel network experiences a serious over-the-limit problem as the distribution network line length increases and PV access capacity becomes larger (Figure 5).

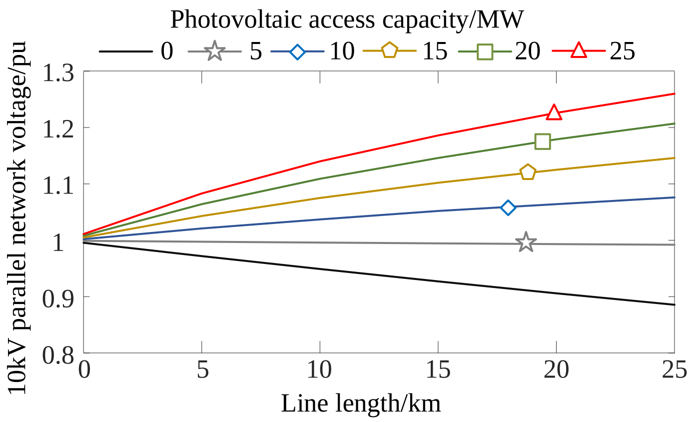

Figure 5. Effects of PV access capacity and line length on line voltage.

Combining Figure 4 and Equation (8), we can determine that the relationship between U_{s0} and 10 kV bus first section voltage U_s after connecting DRPST can be expressed as:

$$\begin{cases} \Delta U_z = \frac{P_i R_{DRPST} + Q_i X_{DRPST}}{U_s - U_{DRPST}} \\ U_{s0} = U_s(1 - k\cos\alpha) - \sum\limits_{i=1}^{N} \Delta U_z \end{cases}, \quad (11)$$

where U_z is the voltage drop formed by the resistance inside DRPST. From Equation (11), DRPST can achieve continuous regulation of its string line voltage while only adjusting its stator–rotor relative angle and then controlling the access point voltage U_{s0}. It exhibits the advantages of simple control and high stability compared with the traditional reactive power–control voltage compensation mode.

To realize the optimization of DRPST voltage regulation–loss reduction in multiple zones of active distribution networks while exhibiting nondifferential control characteristics, a two-layer optimization model with a recursive structure is proposed. In this model, the inner model solution is based on the establishment of the outer decision variables, while the optimization objective of the outer layer depends on the optimal solution of the inner model [17]. As indicated in Equations (10) and (11), access to DRPST can effectively solve the problem of voltage crossing limits at the end of the line. However, the line loss problem should be considered under the premise of guaranteeing voltage deviation. For the actual problem, the lowest voltage deviation and the minimum line loss are chosen as the objectives of the inner model proposed in the current study, while the DRPST rotor angle position is the objective of the outer model. Then, the DRPST real-time rolling voltage regulation model is constructed by considering line loss based on the two-layer planning theory.

3.2. Inner Layer Model That Considers Voltage Control and Line Loss

3.2.1. Objective Function

Voltage Deviation Target

The objective function of the co-ordinated voltage optimization control of the distribution network is to minimize total voltage deviation at each node, i.e., to minimize the time-series average of the normalized voltage deviation sum of squares at each 10 kV parallel network within the optimization cycle.

Simultaneously, the voltage deviation target of each 10 kV parallel network should be graded by considering the importance of the load [18], including three categories (Levels 1, 2, and 3). The corresponding weights are assigned as 0.5, 0.3, and 0.2, respectively. After quantifying the load on each parallel network, we can obtain:

$$F_1 = \min \Delta U = \sum_{i=1}^{N} \omega_{si} L_{si} \left(\frac{U_{si} - U_{si}^*}{U_{simax} - U_{simin}} \right)^2, \quad (12)$$

where U_{si} is the voltage magnitude of system node i; U_{si}^* is the reference voltage magnitude of node voltage i, and it is typically 1.0 (the standard lowest value); U_{simax} is the maximum allowable voltage of node i; U_{simin} is the minimum allowable voltage of node i; ω_{si} is the weight of the load of node i; and L_{si} is the power of the load of the node.

Line Loss Target

Under the premise of guaranteeing system security and power quality, the lowest line loss should be considered comprehensively, and the current study primarily considers the power loss S_{sGi} from the substation to the distributed power access node. The overall line loss target at that moment can be expressed as follows:

$$F_2 = \min S = \sum_{i=1}^{3} \frac{(P_L - P_{DG})^2 + (Q_L - Q_{DG})^2}{U_{si}^2} (R_i + jX_i), \quad (13)$$

The reasonable adjustment of the size of U_{si} can reduce distribution network loss under the premise that PV access capacity and distribution network line length remain unchanged.

3.2.2. Binding Conditions

(1) Voltage deviation constraint: in accordance with "power quality supply voltage deviation" [19], voltage deviation limits that are allowed to pass through the lines of various voltage levels are different, with the voltage deviation limit for the parallel network voltage constraint.
(2) DRPST equivalent voltage source magnitude phase angle constraint.
(3) Power equivalence constraint.
(4) Branch current constraint: to prevent the long-term overcurrent operation of the line from causing permanent damage to the line, i.e., the line carrying capacity for constraint.
(5) Calculation time constraint: the application scenario of this study belongs to an online calculation scenario and, thus, the calculation time of the control variable U_{DRPST} is constrained. When calculation time exceeds sampling time, the current U_{DRPST} value is directly outputted to the outer model.

$$\begin{cases} U_{si}{}^*(1-\varepsilon) \le U_{si} \le U_{si}{}^*(1+\varepsilon) \\ U_{\mathrm{DRPST}}^{\min} \le U_{\mathrm{DRPST}} \le U_{\mathrm{DRPST}}^{\max} \\ \delta_{\mathrm{DRPST}} = \delta_{\mathrm{s}} \\ P_i = U_i \sum U_j (G_{ij}\cos\theta_{ij} + B_{ij}\sin\theta_{ij}) \\ Q_i = U_i \sum U_j (G_{ij}\cos\theta_{ij} - B_{ij}\sin\theta_{ij}) \\ |I_i| \le I_{\max} \\ t \le \eta \end{cases}, \tag{14}$$

3.3. Outer-Layer Model of DRPST-Based Deviation-Free Control

The outer model essentially represents the problem of solving the angle of the DRPST rotor. To ensure the nondifferential control of the angle of the DRPST rotor, a double closed-loop PI control method is adopted. The value of U_{DRPST} calculated by the inner model is set as the target of voltage inner loop control. From the value in Equation (8), a speed-limiting module is adopted in the angle's outer loop control. The output of the actual α value can realize the function of voltage regulation.

4. DRPST Control Strategy

4.1. Solution Strategy for the Inner-Layer Model

In multi-objective optimization problem solving, the optimal solution is a set of solutions wherein the value of any one objective function can no longer be optimized further without degrading the other objective functions. The solution of a multi-objective optimization problem is not unique, but a set of Pareto optimal solutions is available and no comparability occurs between solution sets. A certain objective of the solution may be optimal, while another objective may be weaker than the other solutions. The decision maker can select one solution or part of the solution from the Pareto optimal solution set as the final solution for the requested multi-objective optimization problem in accordance with the requirements of the actual problem and the convenience of operation [20].

In the current study, a multi-objective PSO (MOPSO) algorithm is used to solve the inner model [21], wherein individual particles consist mostly of position and velocity parameters:

$$\begin{cases} v_{i+1} = \omega v_i + c_1 r_1 (pbest_i - x_i) + c_2 r_2 (gbest_i - x_i) \\ x_{i+1} = x_i + v_{i+1} \end{cases}, \tag{15}$$

where ω is the inertia weight, v_{i} is the i-th particle velocity vector, c_1 and c_2 are the acceleration factors, r_1 and r_2 are the random numbers that are uniformly distributed in the interval [0, 1], v_{i} is the i-th particle velocity vector, $p_{\mathrm{best}i}$ is the individual optimal position of the i-th particle, x_i is the position vector of the i-th particle, and g_{besti} is the individual optimal position of the i-th particle.

To meet the demand of an online operation scenario and improve the efficiency of the MOPSO solution, the traditional MOPSO is improved and dynamic parameters are designed for the inertia weights and acceleration factors in the solution.

$$\begin{cases} \omega = \omega_{\max} - \frac{\omega_{\max} - \omega_{\min}}{N_{\max}} N \\ c_1 = c_{\max} - \frac{c_{\max} - c_{\min}}{N_{\max}} N \\ c_2 = c_{\min} + \frac{c_{\max} - c_{\min}}{N_{\max}} N \end{cases}, \tag{16}$$

where $\omega_{\min}$ and $\omega_{\max}$ are the minimum and maximum values of inertia weights, respectively; c_1 and c_2, $c_{\min}$, and $c_{\max}$ are the current, minimum, and maximum values of learning factors, respectively; N is the current number of iterations; and $N_{\max}$ is the maximum number of iterations. The initial stage of the algorithm ω is larger and, thus, beneficial for the global search of the algorithm. The later iteration of ω is gradually reduced, which is favorable for the local search of the algorithm. In the beginning of the iteration, c_1 is larger and c_2 is smaller. This condition is beneficial for the recognition of individuals by particles. Later in the iteration, c_1 is smaller, while c_2 is larger, and a particle demonstrates strong cognitive ability for global search [22].

4.2. Selection of the Optimal Compromise Solution for the Inner Model

The fuzzy affiliation function method [23] is used to express the degree of satisfaction that corresponds to each objective function in the Pareto solution set and, thus, select the optimal compromise solution. The fuzzy affiliation function is defined as:

$$\mu_i = \begin{cases} 1, & f_i < f_{i\min} \\ \frac{f_{i\max} - f_i}{f_{i\max} - f_{i\min}}, & f_{i\min} < f_i < f_{i\max} \\ 0, & f_{i\max} < f_i \end{cases}, \tag{17}$$

where f_{i} is the i-th objective function value and $f_{i\min}$ and $f_{i\max}$ are the upper and lower bounds of the objective function, respectively, during which the maximum value of the standardized satisfaction is solved using Equation (17), i.e., the optimal compromise solution of the inner-layer model [24,25].

$$\mu = \frac{1}{\mathrm{m}} \sum_{i=1}^{\mathrm{m}} \mu_i, \tag{18}$$

where u is the standardized satisfaction value and m is the number of objective functions to be optimized.

4.3. DRPST Control Block Diagram

The overall control block diagram of the DRPST system developed in this study is presented in Figure 6. The specific control process after the device is put into operation is described as follows:

Step 1: The distribution network parameters are inputted. The network voltage parameters are collected. The objective function, constraints, and other distribution network model parameters are set.
Step 2: The parameters of the MOPSO algorithm are initialized.
Step 3: Particle positions, particle velocities, and external profiles are randomly initialized.
Step 4: The objective function of each particle is calculated and the nondominated solution is stored in the external file.
Step 5: The current inertia weights and acceleration factors, particle positions, velocities, individual optimal positions, and global optimal positions are updated in accordance with Equation (16).
Step 6: The external archive is updated with the current particle swarm nondominated solution.
Step 7: Whether the current time exceeds the maximum sampling time is recorded. Step 9 is skipped if it does. Proceed to Step 8 if it does not.

Step 8: The size of the current iteration number is compared with the maximum iteration number. If the two are equal, then proceed to Step 9.
Step 9: Searching is stopped. The external file is the Pareto optimal solution set. Pareto solution set satisfaction is calculated from Equations (17) and (18). The optimal compromise solution and the current control variables are outputted.
Step 10: The control variable U_{DRPSTref} in Step 9 is used as the outer model set value. A difference is made with the current U_{DRPST} and the nondifferential control of the voltage set value is realized by the PI controller.
Step 11: Using the solution of Step 10 U_{DRPST}, the rotor angle α_{DRPST} is set by solving Equation (8) for the output DRPST. A difference is made with the actual angle α_{DRPST} to achieve the nondifferential control of the angle set value.
Step 12: Real-time rolling optimization of DRPST is achieved based on the parallel network voltage obtained from the next period of rolling acquisition.

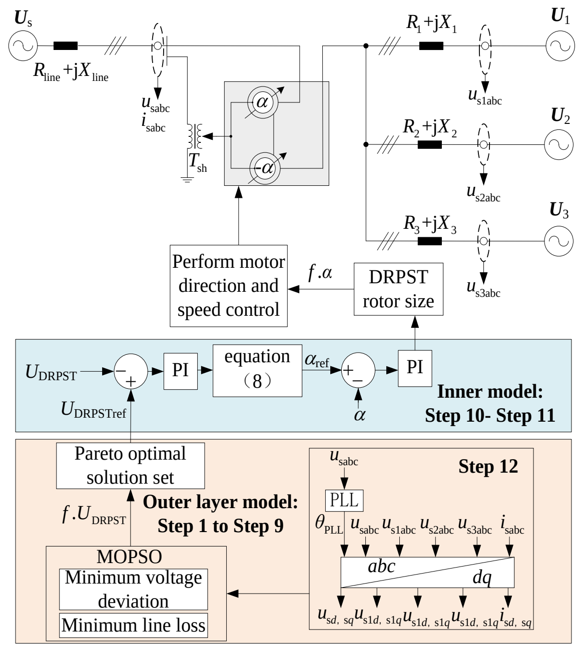

Figure 6. Block diagram of the overall system control of DRPST.

5. Simulation Analysis

5.1. Design of System Parameters

To verify the effectiveness of the proposed topology and control strategy, a specific distribution network model is built in MATLAB/Simulink based on the grid structure shown in Figure 6. The relevant parameters are provided in Table 1. The relevant parameters of the MOPSO algorithm are listed in Table 2.

Table 1. Distribution network and DRPST device parameters.

Parameters	Value	Parameters	Value	Parameters	Value
Frequency/Hz	50	Capacity/MW	3	Rotational speed	20°/s
$\boldsymbol{U}_s$/kV	10∠0°	Z_{sh}/Ω	0.3	Station area 1 load level	Level 1
$R_1 + jX_1/\Omega$	2.61 + j2.134	Z_{RPST}/Ω	0.15	Station area 2 load level	Level 2
$R_2 + jX_2/\Omega$	2.7 + j2.208	$R_3 + jX_3/\Omega$	2.025 + j1.656	Station area 3 load level	Level 3

Table 2. Basic parameters of MOPSO.

Parameters	Value	Parameters	Value	Parameters	Value
Number of iterations	50	c_{max}	0.2	ω_{max}	0.5
Population size	100	c_{min}	0.1	ω_{min}	0.001
External population file size	100	v_{max}	1.2	v_{min}	0.8

From the analysis of the DRPST regulation range in accordance with the parameters in Table 1, the relationship characteristics between the first section voltage of the system and the rotor angle of DRPST under the current simulation parameters are illustrated in Figure 7. When the rotor angle of DRPST $\alpha = 0°$, the voltage of DRPST injected into the line exhibits the maximum value. Meanwhile, the voltage phase of DRPST injected into the line always remains the same with the original transmission line.

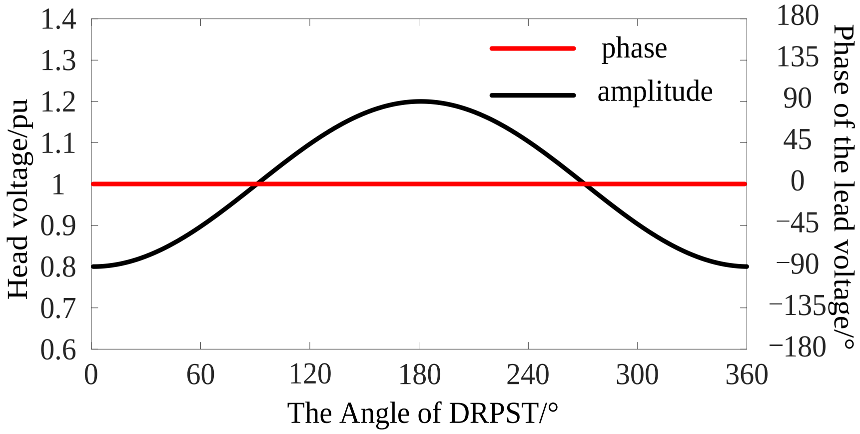

Figure 7. Adjustment range of DRPST.

5.2. Simulation Verification of Steady-State Regulation Characteristics

PV power generation is closely related to a variety of meteorological factors and subject to their constraints. Thus, to verify the steady-state regulation characteristics of DRPST, the 24 h DRPST regulation effect is simulated. The 24 h PV output and load power curves are shown in Figure 8 [26]. The comparison of voltage and network-wide line loss of each station area before and after adding DRPST is illustrated in Figure 9.

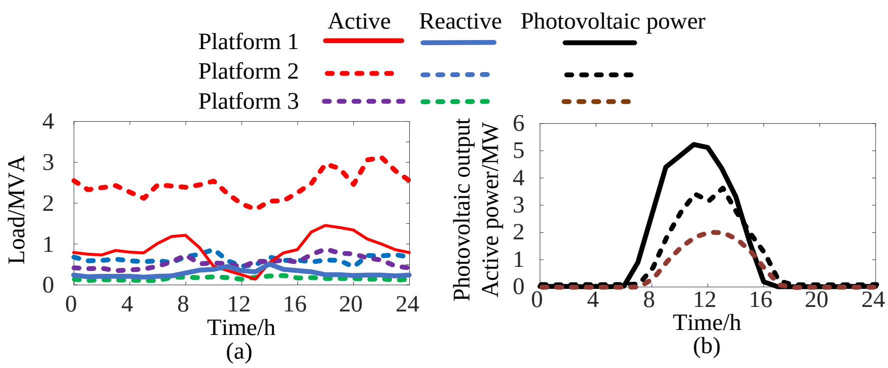

Figure 8. 24 h PV output and load curve. (**a**) Variation of station load in 24 hours. (**b**) The change of photovoltaic output in 24 h.

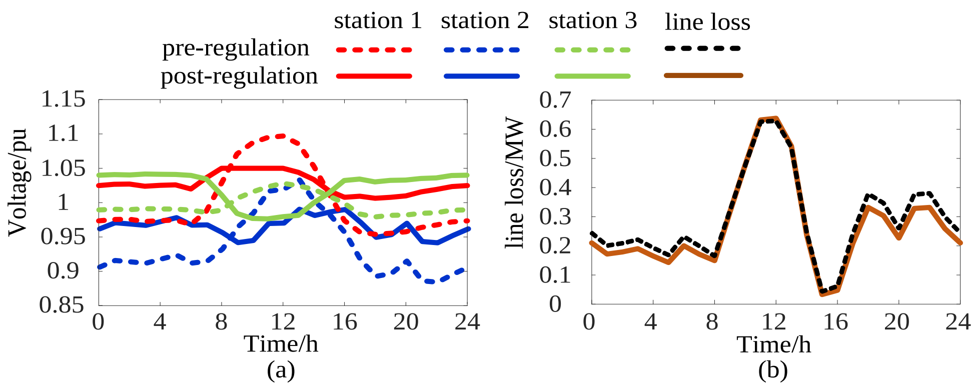

Figure 9. Connection point voltage and system grid loss before and after adding DRPST. (**a**) Voltage change of each station area after DRPST is connected. (**b**) Network loss changes after DRPST is connected.

From Figure 9a, the voltage overrun phenomenon of distribution station areas 1 and 2 is effectively improved after accessing DRPST. However, considering that the voltage deviation target model is for the total voltage deviation of each node time series squared and minimized, the worse voltage performance of the parallel network (although still within the voltage deviation constraint) is recorded under the premise that the load level of distribution station area 3 is lower and electricity consumption is less. As shown in Figure 9b, line loss is effectively reduced after accessing DRPST, and the economic operation level of the distribution network is improved.

5.3. Simulation Verification of Transient Regulation Characteristics

PV output power depends on the distribution of solar irradiance, and solar radiation received by PV power generation units is easily affected by weather type; hence, the distribution network model of the temporary rise/fall of PV power generation caused by cloud movement under cloudy weather conditions is designed. Subsequently, the DRPST control characteristics are simulated and verified.

To verify the DRPST control characteristics, the 14:00 data in Figure 9 are selected for simulation, as indicated in Table 3. DRPST is put into operation at the moment of 0 s. At the moment of 15 s, the sudden drop in PV output is caused by the cloud blocking solar radiation. Furthermore, the load is set to change at the moment of 30 s to verify the regulation ability of DRPST under a sudden change in load.

Table 3. Parameters of load output and PV output change in each station area.

Parameters	t = 0 s	t = 15 s	t = 30 s	Parameters	t = 0 s	t = 15 s	t = 30 s
Station area 1 load/MVA	0.55 + j052	0.55 + j052	0.87 + j0.39	PV for station area 1/MW	3.32	0.66	0.66
Station area 2 load/MVA	2.05 + j0.68	2.05 + j0.68	2.26 + j0.60	PV for station area 2/MW	2.71	0.41	0.41
Station area 3 load/MVA	0.56 + j0.21	0.56 + j0.21	0.55 + j0.22	PV for station area 3/MW	1.75	0.44	0.44

Figure 10a–c, show the Pareto solution set and the optimal compromise solution of the outer model at t = 0, 15, and 30 s. Figure 10d shows the whole process of the inner-loop control of voltage and outer-loop control of angle for the inner model. Figure 10e–g depict the dynamic change in voltage at the parallel network of each station. The comparison effect before and after the improvement of the MOPSO algorithm is illustrated in Figure 11.

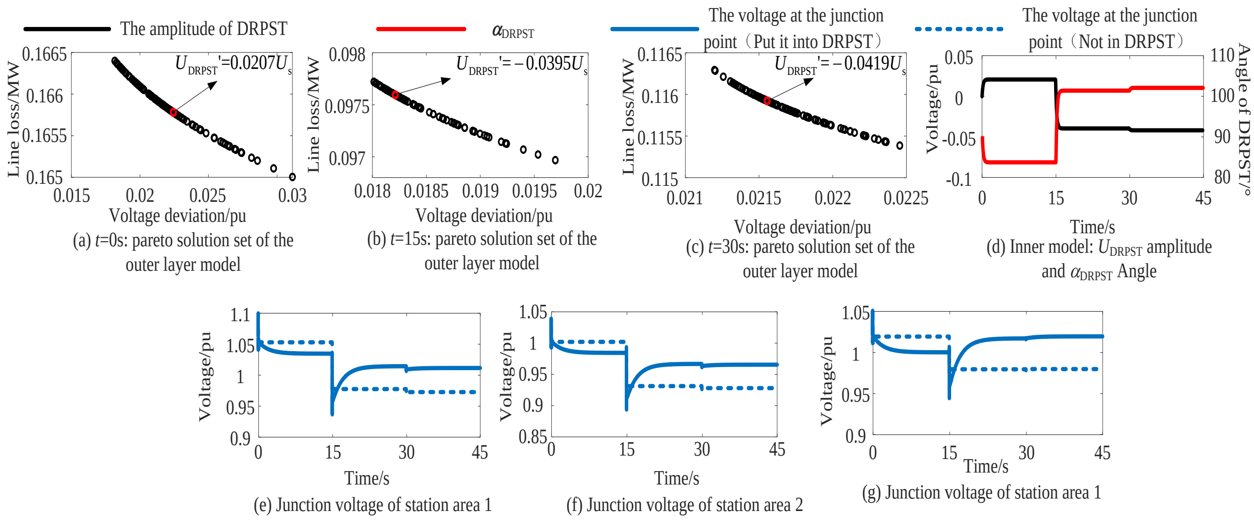

Figure 10. DRPST control process and simulation results.

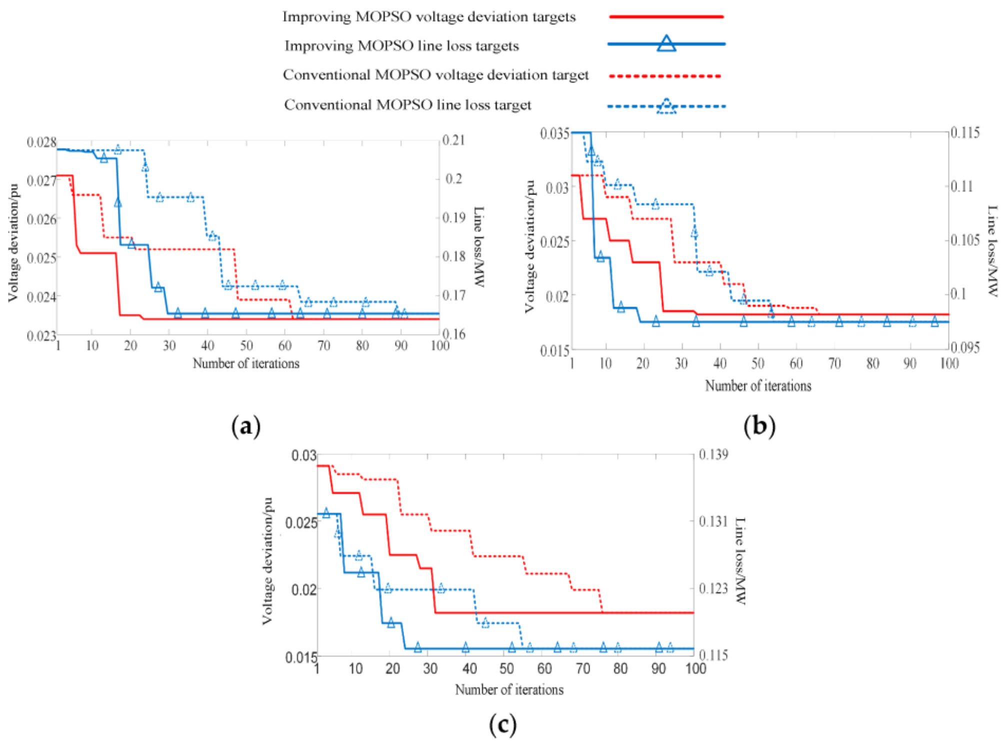

Figure 11. The process of solving multi-objective particle swarm algorithm before and after improvement. (**a**) Optimization search process for t = 0 s. (**b**) Optimization search process for t = 15 s. (**c**) Optimization search process for t = 30 s.

DRPST can always output the corresponding compensation voltage when a transient rise/fall in voltage occurs at the end of the line. The response time is in seconds, such that the voltage of each station area is always within the range of voltage deviation. On this basis, As can be seen from Figure 11, compared with the traditional MOPSO, the dynamic parameter design of inertia weights and acceleration factors in the solution process can effectively improve the solution speed and meet the online operation requirements.

6. Experimental Validation of DRPST

Experimental Platform Construction

In the experimental design, mostly for validating DRPST topology and its control strategy, a 380 V/40 kVA experimental prototype of DRPST is developed. The main part of this prototype consists of two sets of variable ratio 380:100. The capacity of the rotating transfer phase transformer is 20 kVA. The control module adopts a digital signal processor (DSP) controller. The servo motor speed is 2400 rpm, which is attributed to RPST's rotor side speed of 6°/s. The DRPST experimental platform is shown in Figure 12. The system parameters are provided in Table 4.

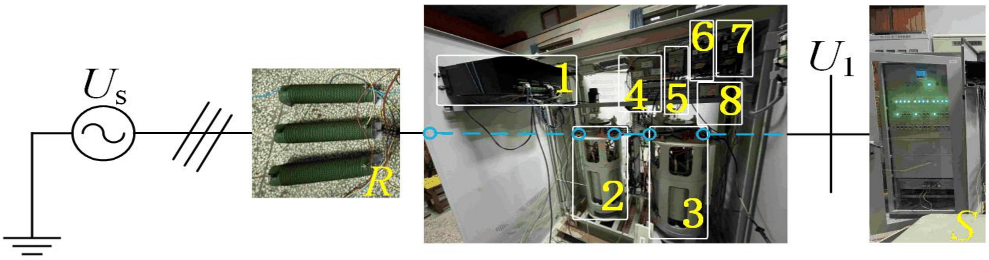

Figure 12. Experimental platform of DRPST. (1) is the DSP controller. (2) and (3) are the two RPST main structures. (4) is the current transformer. (5) is the RPST energy side input switch, which is automatically closed when the power supply generates excitation to the stator windings, and automatically disconnected when the excitation is cancelled. (6) is the DRPST series switch k_{ss}. (7) is the DRPST bypass switch k_{bp}. (8) is the RS485 interface.

Table 4. Parameter design of the experimental system.

Parameters	Value	Parameters	Value	Parameters	Value
U_s/V	380	Capacity/kVA	40	Stator–rotor ratio	380:100
Frequency/Hz	50	S/kVA	1.1 + j0.5	R/W	5

In the figure, 1 is the DSP controller; 2 and 3 are two groups of RPST main structure; 4 is the current transformer; 5 is the RPST energy-taking side input switch, which is automatically closed when the power supply generates excitation to the stator winding and automatically disconnected when excitation is canceled; 6 is the DRPST series switch k_{ss}; 7 is the DRPST bypass switch k_{bp}; 8 is the RS485 interface; S is the load box; and R is the resistive element.

In accordance with the regulation characteristics of the device, two experimental conditions are designed to verify its effectiveness and robustness, namely, the variable and constant voltage setting experiments. The experimental condition design is presented in Table 5.

Table 5. Design of experimental conditions

<table>
<tr><td rowspan="2">Experiment (1)/V</td><td>t_0–t_1</td><td>t_1–t_2</td><td>t_2–t_3</td><td>t_3–t_4</td><td>t_4–t_5</td><td>t_5–t_6</td></tr>
<tr><td>220</td><td>200</td><td>185</td><td>260</td><td>240</td><td>220</td></tr>
<tr><td rowspan="2">Experiment (2)/kVA</td><td>t_0–t_1</td><td>t_1–t_2</td><td colspan="2">t_2–t_3</td><td>t_3–t_4</td><td>t_4–t_5</td></tr>
<tr><td>uninvested</td><td>1.1 + j0.5</td><td colspan="2">3.3 + j1.8</td><td>3.3 + j0.6</td><td>2 + j1.5</td></tr>
</table>

(1) Variable voltage setting experiment

To maintain the same premise, the DRPST string in the line end load and line resistance is adjusted into the line voltage to achieve parallel network voltage bidirectional regulation function through the six-stage experimental conditions to verify its effectiveness and robustness. The experimental waveform is shown in Figure 13.

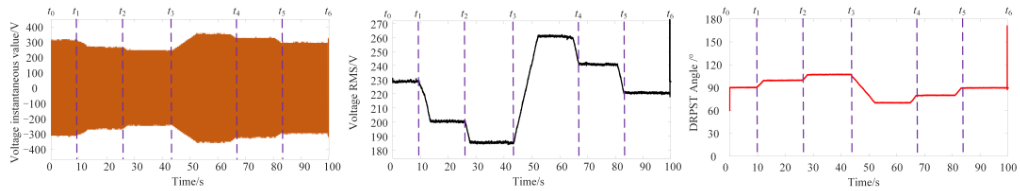

Figure 13. Experiment with variable voltage set point.

(2) Constant voltage setting experiment

Line end load change will lead to changes in the parallel network voltage. The parallel network voltage is set to 220 V. The effect of DRPST regulation at this time is observed. The overall experiment has five stages. The experimental waveform is shown in Figure 14.

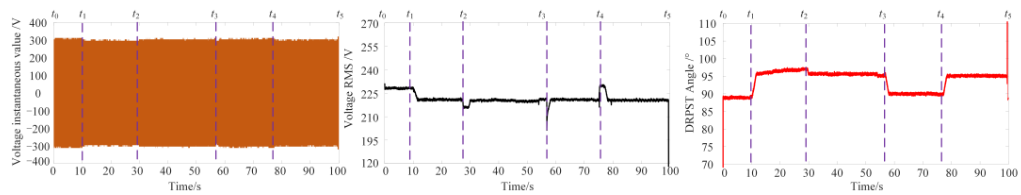

Figure 14. Experiment with constant voltage set point.

DRPST can always provide voltage compensation quickly and effectively to meet voltage regulation requirements under the variable and constant voltage set point experiments. In summary, the experimental results verify the effectiveness and correctness of the proposed DRPST topology and its control strategy.

7. Conclusions

DRPST is proposed to solve the problem of voltage crossing the limit of a parallel network caused by the high proportion of distributed PV access. The following conclusions are drawn through theoretical analysis, simulation, and experimental verification.

(1) In this study, a new regulating structure based on DRPST is proposed. A simplified circuit model of DRPST is constructed, its control characteristics are analyzed, and its regulating performance is verified through experiments. DRPST string-in line voltage is only affected by rotor angle. The constructed model exhibits the advantages of bidirectional continuous voltage regulation and simple control.
(2) A two-layer optimization model and its control strategy are proposed for the optimization of voltage regulation and loss reduction in multiple-zone active distribution networks.
(3) DRPST is an electromagnetic voltage regulator that exhibits better shock resistance and reliability than power electronic voltage regulators. The generated loss and harmonic content will be considerably reduced. Manufacturing, operation, and maintenance costs are relatively low, providing an effective complement to future active distribution network voltage regulation schemes.

Author Contributions: Conceptualization, C.S., X.Y. and J.J.; Methodology, C.S., X.Y., W.A. and J.J.; Validation, C.S., Y.Y., W.A. and J.J.; Formal analysis, C.S., X.Y., W.A., J.J. and J.L.; Investigation, C.S., Y.Y., W.A. and J.L.; Resources, X.Y. and J.L.; Data curation, C.S., Y.Y. and J.J.; Writing—original draft, C.S.; Writing—review & editing, C.S., X.Y., Y.Y. and J.J.; Supervision, X.Y. and J.J.; Project administration, X.Y., W.A. and J.J.; Funding acquisition, X.Y. All authors have read and agreed to the published version of the manuscript.

Funding: This research was funded by (1) Science and Technology Project of Baoding, China (NO. 2211ZG015); (2) Scientific Research Project of Colleges and University in Hebei Province, China (NO. ZC2023047).

Institutional Review Board Statement: Not applicable.

Informed Consent Statement: Not applicable.

Data Availability Statement: Data is contained within the article.

Conflicts of Interest: The authors declare no conflict of interest.

References

1. Zhong, Y.; Ji, L.; Jiang, Y.; Li, J.; Wang, Z.; Wang, Y. Fine-grained Calculation Method of Accepting Distributed Generation Capacity in Distribution Network for Virtual Power Plant. In Proceedings of the 2023 IEEE 6th International Electrical and Energy Conference (CIEEC), Hefei, China, 12–14 May 2023; pp. 159–164.
2. Lin, Z.Y.; Jiang, F.; Tu, C.; Xiao, Z. Distributed Coordinated Voltage Control of Photovoltaic and Energy Storage System Based on Dynamic Consensus Algorithm. In Proceedings of the 2021 IEEE/IAS Industrial and Commercial Power System Asia (I&CPS Asia), Chengdu, China, 18–21 July 2021; pp. 1223–1228.
3. Navarro-Espinosa, A.; Ochoa, L.F. Increasing the PV hosting capacity of LV networks: OLTC-fitted transformers vs. reinforcements. In Proceedings of the 2015 IEEE Power & Energy Society Innovative Smart Grid Technologies Conference (ISGT), Washington, DC, USA, 18–20 February 2015; pp. 1–5.
4. Liu, X.; Niu, X.S.; Zhu, Y.; Zhu, C. Influence of Regulation of OLTC Transformation Ratio on Voltage Stability. In Proceedings of the 2013 Fourth International Conference on Digital Manufacturing & Automation, Shinan, China, 29–30 June 2013; pp. 696–700.
5. Zhang, L.; Zhu, Y.; Xiao, Y. Voltage Segment Coordinated Control Strategy for Isolated DC Microgrid with Multiple Energy Storage Units. In Proceedings of the 2019 22nd International Conference on Electrical Machines and Systems (ICEMS), Harbin, China, 11–14 August 2019; pp. 1–5.
6. Weber, H.; Baskar, P.; Ahmed, N. Nodal Voltage Angle Control of Power Systems with Renewable Sources, Storages and Power Electronic Converters. In Proceedings of the 2018 International Conference on Smart Energy Systems and Technologies (SEST), Seville, Spain, 10–12 September 2018; pp. 1–6.
7. Ba, A.O.; Peng, T.; Lefebvre, S. Rotary Power-Flow Controller for Dynamic Performance Evaluation—Part I: RPFC Modeling. *IEEE Trans. Power Deliv.* **2009**, *24*, 1406–1416. [CrossRef]
8. Ba, A.O.; Peng, T.; Lefebvre, S. Rotary Power Flow Controller Performance in Power Systems Part I—RPFC Modeling. In Proceedings of the IEEE International Symposium on Industrial Electronics, Cambridge, UK, 30 June–2 July 2008.
9. Tan, Z.; Zhang, C.; Jiang, Q. Research on Characteristics and Power Flow Control Strategy of Rotary Power Flow Controller. In Proceedings of the 5th International Youth Conference on Energy (IYCE), Pisa, Italy, 27–30 May 2015.
10. Abardeh, M.H.; Ghazi, R. Rotary power flow controller (RPFC) characteristics analysis. In Proceedings of the 2011 5th International Power Engineering and Optimization Conference, Shah Alam, Malaysia, 6–7 June 2011; pp. 358–363.
11. Li, T.; Wu, H.; Chen, H. Based on Deep Reinforcement Learning Algorithm, Energy Storage Optimization and Loss Reduction Strategy for Distribution Network with High Proportion of Distributed Generation. In Proceedings of the 2023 8th Asia Conference on Power and Electrical Engineering (ACPEE), Tianjin, China, 14–16 April 2023; pp. 1863–1868.
12. Yu, W.; You, R.; Zhou, J. Research on Operation Optimization of Active Distribution Networks Based on Multi-Port SOP Integrated Energy Storage System. In Proceedings of the 2021 6th International Conference on Power and Renewable Energy (ICPRE), Shanghai, China, 17–20 September 2021; pp. 707–712.
13. Lu, L.; Liu, J.; Wang, J. A distributed hierarchical structure optimization algorithm based poly-particle swarm for reconfiguration of distribution network. In Proceedings of the 2009 International Conference on Sustainable Power Generation and Supply, Nanjing, China, 6–7 April 2009; pp. 1–5.
14. Ba, A.O.; Peng, T.; Lefebvre, S. Rotary Power-Flow Controller for Dynamic Performance Evaluation—Part II: RPFC Application in a Transmission Corridor. *IEEE Trans. Power Deliv.* **2009**, *24*, 1417–1425. [CrossRef]
15. Peng, T.; Ba, A.O.; Lefebvre, S. Rotary power flow controller performance in power systems part II—RPFC performances in a transmission corridor. In Proceedings of the 2008 IEEE International Symposium on Industrial Electronics, Cambridge, UK, 30 June–2 July 2008; pp. 1476–1482.
16. Yan, X.; Shao, C.; Peng, W. Flexible Loop Closing and Emergency Power Control Method for Active Distribution Network Based on the Rotary Power Flow Controller. *Proc. Chin. Soc. Electr. Eng.* **2023**, *43*, 6192–6204.
17. Ba, A.O.; Peng, T.; Lefebvre, S. Rotary Power Flow Controller modeling for dynamic performance evaluation. In Proceedings of the 2008 IEEE Power and Energy Society General Meeting-Conversion and Delivery of Electrical Energy in the 21st Century, Pittsburgh, PA, USA, 20–24 July 2008; pp. 1–10.
18. Shang, L.; Hu, R.; Wei, T.; Ci, H.; Zhang, W.; Chen, H. Multiobjective optimization for hybrid AC/DC distribution network structure considering reliability. In Proceedings of the 2021 IEEE Sustainable Power and Energy Conference (iSPEC), Nanjing, China, 23–25 July 2021; pp. 3034–3041.

19. *IEEE Std C57.12.80-2010*; IEEE Standard Terminology for Power and Distribution Transformers. Revision of IEEE Std C57.12.80-2002; IEEE Standard Association: Piscataway, NJ, USA, 2010; pp. 1–60. [CrossRef]
20. Li, L.; Gao, M.; Gan, L.; Li, W.; You, G.; Tao, Z.; Wang, J. Two-level Capacity Optimization Strategy for Generations in Multi-energy Gathering Center Considering the Flexibility. In Proceedings of the 2020 IEEE 4th Conference on Energy Internet and Energy System Integration (EI2), Wuhan, China, 30 October–1 November 2020; pp. 2599–2604.
21. Su, W.; Xiao, X.; Yang, X.; Fang, X. Research on distribution network expansion planning based on load feature library and load simultaneous rate. In Proceedings of the 2022 IEEE 10th Joint International Information Technology and Artificial Intelligence Conference (ITAIC), Chongqing, China, 17–19 June 2022; pp. 1471–1475.
22. Zhao, L.; He, D.; Zeng, X.; Wu, J. Distributed Photovoltaic Energy Storage Configuration Method for Distribution Network Considering Voltage Constraint. In Proceedings of the 2023 IEEE 3rd International Conference on Information Technology, Big Data and Artificial Intelligence (ICIBA), Chongqing, China, 26–28 May 2023; pp. 485–489.
23. Ren, C.; Zhou, J.; Xu, X.; Mao, W.; Ma, Y.; Wang, B. Load Balance and Recovery Optimization of Distribution Network Based on Binary Particle Swarm Optimization Algorithm. In Proceedings of the 2022 5th International Conference on Renewable Energy and Power Engineering (REPE), Beijing, China, 28–30 September 2022; pp. 103–107.
24. Zhang, M.J.; Zhang, Z.Y.; Yi, H.; Tang, X. Demand Response Featured Dynamic Voltage Regulation of Active Distribution Network. In Proceedings of the 58th IEEE/IAS Industrial and Commercial Power Systems Technical Conference Asia (IEEE I and CPS Asia), Shanghai, China, 8–11 July 2022.
25. Zhou, S.C.; Zhou, Y.P.; Wei, Y.C.; Kang, L.; Zhang, X. Multi-Objective Optimal Control for Distribution Network Loop-Closing Operation Using PE-MOPSO Algorithm. In Proceedings of the 6th International Conference on Smart Grid and Electrical Automation (ICSGEA), Kunming, China, 29–30 May 2021.
26. Zogg, R.; Lawrence, T.; Ofer, D. Distributed Energy Storage. *Ashrae J.* **2007**, *49*, 90.